

Development of Nanostructured Solid Oxide Fuel Cell Electrodes

G. Schiller*, A. Ansar, D. Soysal,

Deutsches Zentrum für Luft- und Raumfahrt (DLR), Institut für Technische

Thermodynamik, Pfaffenwaldring 38-40, D- 70569 Stuttgart, Germany

*Fax: +49 711 6862 747, E-mail: guenter.schiller@dlr.de

Abstract

Nanostructured coatings have been fabricated for use as electrodes in solid oxide fuel cells (SOFC) by developing and applying innovative plasma spraying methods. Nanostructured cathode coatings of a variety of chemical composition were fabricated by thermal plasma chemical vapor deposition (TPCVD) using a RF plasma torch. Deposits of desired phase and microstructure were successfully produced. The cathode layers exhibited initially undesired secondary phases but this could be overcome by adjusting the chemical composition of the precursors. The microstructure of the deposited cathode was columnar-type with very high open porosity and specific surface area. The nanostructured NiO+YSZ anodes have been fabricated by three means: spraying of pre-synthesized agglomerates of nanoparticles, suspension dc plasma spraying and solution precursor dc plasma spraying. The nanostructured anode fabricated by pre-synthesized agglomerates of nanoparticles exhibited better gas permeability, comparable high temperature conductivity, and 43% lower polarization in SOFC operation at 800 °C compared to conventional anodes. Moreover, by controlling the electrode structure, the anode nanostructure could be maintained for 1500 hours of operation. Further improvement in the microstructure of anodes is in progress using dc plasma suspension and solution precursor spraying.

Key words: Solid oxide fuel cells, nanostructured cathode, nanostructured anode, manufacture of electrodes, suspension and solution precursor plasma spraying, electrochemical performance

Introduction

Solid oxide fuel cells (SOFC) considered as highly efficient and environmentally friendly energy converters, convert chemical energy from fuel and oxidizing gases directly into electrical energy and heat [1]. The basic components of a SOFC cell consist of the porous electrodes - an anode for fuel supply and a cathode for air supply - which are separated by a gastight oxygen ion conductive electrolyte layer. The electrolyte usually consists of doped zirconia or ceria. A cermet of yttria-stabilized zirconia (YSZ) and nickel is mostly used for the anode and perovskite-type oxides such as doped lanthanum manganite (LSM), lanthanum cobaltite and ferrite (LSC, LSF, LSCF) are the common materials for the cathode [2]. The electrodes have to provide the reaction sites for the oxidation of the fuel gas at the anode and for the reduction of oxygen molecules at the cathode. Ohmic, activation and concentration polarizations control collectively the performance of SOFCs. The resistivity in the electrolyte shows the main contribution to ohmic polarization. Activation polarization is dependent on the electrodes-electrolyte interface and is controlled by charge transfer processes. Transport of gases (fuel and oxidizing gas) through electrodes governs concentration polarization. In case of thin film electrolyte cells it has been observed that despite low ohmic polarization the area specific resistance (ASR) of the cell could be several times larger which is due to a significant influence of activation and concentration polarizations [3]. As suggested by different authors [4, 5], activation polarization can be effectively decreased by enhancing the electrochemical

reaction zones, i.e. the triple phase boundaries (TPBs) formed at the interface of YSZ, Ni and fuel gas in the anode and at the interface of YSZ, LSM and oxygen in the cathode. Electrodes having a microstructure that facilitates easy flow and homogeneous distribution of gases exhibit lower concentration polarization [6]. Significant improvement in electrode performance can be attained by introducing nanostructured materials which can increase substantially the specific surface area and TPBs. However, tailoring the microstructure can be a challenge as the porosity and pore size needs to be adjusted to keep the concentration polarization limited. Additionally, several researchers have reported an increase of multiple orders of magnitude in the electronic and ionic conductivity at elevated temperatures for the nanocrystalline ceramics compared to solids having micrometric sized grains [7, 8].

Plasma spraying is one of the promising techniques to develop nanostructured functional layers for SOFC. It offers distinct advantages in terms of short fabrication time for the deposits, simple automation and up-scalability. In conventional plasma spraying, feedstock materials such as powders, wires etc, are introduced in a plasma jet using a gas carrier. In the plasma, the particles are heated and accelerated simultaneously towards a prepared substrate. Impingement, flattening and solidification of impacted particles on the surface of a substrate results in lamellar structures called splats. Consolidation of splats leads to the construction of a deposit [9, 10]. The microstructure and quality of the deposit depends on splat morphology and intersplat contact nature which are influenced by substrate surface conditions (temperature, roughness, chemical state, etc) [11] as well as impacting particle properties (temperature, velocity, Reynolds number (Re) and Weber number (We)) [12]. Feedstock and the operating conditions of the plasma govern the in-flight properties of particles at impact. As the deposit is generated by random impact of

particles on the substrate microstructural control can be challenging. Additionally, feedstock material needs to have a momentum comparable to that of plasma gases at the injection for proper in-flight particle treatment. This is severe to fulfill for nanosized feedstock as the lower mass of particles needs to be compensated by higher velocities which tend to be too high for a stable plasma. Our team is working towards developing innovative plasma spraying approaches to fabricate nanostructured coatings; an overview of these activities is described in this paper.

Nanostructured cathodes using RF-TPCVD

A promising approach for the preparation of SOFC components such as porous cathode layers is given by the in situ synthesis and deposition in an inductively coupled radio frequency (RF) plasma from liquid precursors. Using suspensions as well as aqueous solutions of suitable salts, the two methods called RF-suspension plasma spraying (SPS) [13] and thermal plasma chemical vapor deposition (TPCVD) [14], have been developed for the deposition of SOFC components. The experiments were performed using a vacuum reactor and a PL50 induction plasma torch from TEKNA Plasma Systems, Sherbrooke/Canada which is operated with a radio frequency generator from Himmelwerk, Germany, at 500 kHz. The RF power was varied in the range from 20 to 30 kW, the chamber pressure was between 12 and 38 kPa and the spraying distance was between 150 and 600 mm. The plasma gas composition was varied over a wide range from argon/hydrogen mixtures to plasma mainly consisting of oxygen. The precursors were fed with a rate between 1.5 and 3 ml/min by a peristaltic pump using two channels to avoid pulsing. The material was directly injected into the hot plasma core by means of

a gas-assisted atomizer. Argon flow rates in the range of 2-10 slpm were used to atomize the precursors. The schematic is shown in Figure 1.

Aqueous solutions of metal nitrates of different concentrations were used as precursors for the preparation of perovskite-type cathode coatings by means of TPCVD. A summary of the main precursor solutions applied and the desired synthesis products is given in Table 1. The phase content of the coatings was determined by XRD using a STOE Stadi P diffractometer and MoK_α radiation. Polished cross sections and fracture surfaces were prepared by standard metallographic procedures to study the coating microstructure by optical and scanning electron microscopy (SEM) as well as EDX mapping.

In first experiments, suspension plasma spraying was applied using suspensions of MnO_2 particles in saturated aqueous and ethanolic solutions of La salts. The perovskite was formed as the main phase [13], however, La_2O_3 was also observed as an additional phase in significant extent in the coating. Post-treatment with an 80 % oxygen plasma improved the coating purity but the occurrence of detrimental La_2O_3 which reacts to $\text{La}(\text{OH})_3$ causing severe volume change and destruction of the coating could not completely be suppressed. Furthermore, the coatings exhibit a layered microstructure resulting from impinging molten particles which is known from conventional thermal spraying processes. Although porosity can be affected by the solid content of the suspension, SPS coatings showed a porosity which is too poor for gas migration in SOFC cathodes. Highly porous microstructures of LSM coatings were observed when using the TPCVD process, but the phase purity remained a problem to be solved. A key parameter governing the purity of the coatings appears to be the radial temperature gradient within the plasma jet. When using lanthanum and manganese nitrates (precursors A, B, C), the high temperature along the axis of the jet combined with the high volatility of Mn results

in a non-stoichiometric composition with regard to La and Mn in the central part of the coating on a stationary substrate. The deviations from stoichiometry are larger than the perovskite structure can tolerate, thus, the presence of surplus La causes La_2O_3 to appear in the coating beside the desired LSM phase. The cooler outer regions of stationary substrates were always covered with pure or almost pure perovskite phase. Figure 2 shows an extreme example of the different phase contents obtained in the centre and in the outer region of a stationary substrate.

Scanning of the substrate results in the simultaneous deposition of the two main phases La_2O_3 and LSM. The homogeneity of the perovskite phase could be substantially improved by using precursors with lower lanthanum content, e.g. $\text{La}_{0.5}\text{Sr}_{0.5}\text{MnO}_3$ (precursors B and C) or by replacing lanthanum by praseodymium (precursor D), but a completely single-phase, large area perovskite coating could not be achieved. The synthesis of LSM, LSF (precursor E) and LSCF (precursor F) showed the same tendency concerning the formation of La_2O_3 but to a different extent. A semi-quantitative method was applied to compare the phase purity of different compounds by calculating the percentage of pure perovskite phase from the intensities of the main XRD peaks of the perovskite and La_2O_3 . Table 2 depicts the phase composition of different perovskite layers.

It is concluded that the volatility of the manganese cannot be the only reason for the non-stoichiometric incorporation of the elements into the central part of the perovskite coating. Regarding the melting points of the simple oxides of the considered elements, La_2O_3 and SrO show far higher values than the other oxides of Mn, Fe and Co. This leads to the consideration that clusters of La_2O_3 or La-Sr-oxide might form in the hot zone along the

plasma jet by homogeneous nucleation similar to the observation made in the system with yttria-stabilized zirconia [7]. These clusters might then be deposited and cannot completely be transformed to the perovskite phase due to the limited interdiffusion of Mn, Fe and Co. A break-through concerning phase purity was achieved when using precursors where La is substituted by Pr (precursor H). With the slightly non-stoichiometric composition $\text{Pr}_{0.58}\text{Sr}_{0.4}\text{Co}_{0.2}\text{Fe}_{0.8}\text{O}_3$ (PSCF) absolutely pure perovskite phase could be observed by XRD measurement both in the centre and on the margin of the layer, as can be seen from Figure 3. An explanation of this behavior cannot be given at present and needs further investigation.

The coatings prepared from the precursor solutions A to H show a columnar or cauliflower-like microstructure as it is shown in SEM images of fracture surfaces in Figure 4 which is a result of heterogeneous nucleation of the material on the substrate surface as it is well known from conventional CVD. During growth of the perovskite layer needle-shaped single crystals are initially formed. The substrate is in a temperature range that provides enough surface diffusion of the impinging species. Therefore the needles can coalesce resulting in a columnar growth. The coalesced crystals had a size varying from 90 to 300 nm. The resulting microstructure is of high open directional porosity offering efficient vertical as well as horizontal gas migration paths. This is an ideal microstructure for application as SOFC cathode enabling excellent gas permeability and creating a lot of reaction zones. The deposition of perovskite coatings by means of the TPCVD process from aqueous solutions resulted in growth rates of up to 25 $\mu\text{m}/\text{min}$ on substrates with a size of 25 cm^2 that were scanned with the plasma jet. Depending on the process conditions and the precursor composition approximately 10 to 40 % of the theoretical oxide content of the precursors contributed to the coating growth. With

optimization of the plasma parameters and application of larger substrates the deposition efficiency of the TPCVD process may achieve the range of about 100 $\mu\text{m}/\text{min}$ which is typical for plasma sprayed ceramic coatings.

Nanostructured anodes using agglomerated nanoparticles

One of the methods to fabricate nanostructured anodes consists of spraying nanoparticles agglomerated to coarse powder particles bigger than 10 μm . The feedstock powder was produced by co-precipitation and spray drying of NiO and YSZ having 60 to 40 wt.%. The primary particles had a size of 20 to 80 nm with d_{50} of 60 nm according to calculations from XRD. The agglomerates had a size range of $\sim 50\text{--}100 \mu\text{m}$ (Figure 5 (a)). To produce nanostructured anode deposit this composite powder was co-sprayed along with an agglomerated micro-sized NiO powder. The NiO agglomerates were added to guarantee the percolation of Ni in the anode. Air plasma spraying (APS) with a standard F4-type gun with a V-type 7 mm internal diameter anode nozzle from Medicoat, Switzerland, was employed for the deposition of the anodes. The plasma enthalpy and particle velocity (governing particle dwell time in the plasma) were experimentally adopted to adjust spray parameters in such a way that only partial melting of the surface of agglomerated powder occurred. This resulted in conserving the nanostructure during spraying. Powder carrier gas flow rate was adjusted to maintain a 3° deviation between the plasma and the particle jet axis. The anode deposits were fabricated on porous FeCrMnTi substrates (48 mm in diameter, 1 mm in thickness) from Plansee, Austria. Figure 5 (b) presents the cross section of the nanostructured anode deposit. The as-sprayed deposits had particles ranging from 60 nm to 220 nm measured randomly on several SEM micrographs at 1000-fold magnification. The characteristics of these

nanostructured anodes were compared to our conventional NiO+YSZ anodes. The detail of processing of conventional anodes is described elsewhere [15]. The permeability of the as sprayed and reduced anodes was measured with the pressure drop method where a constant transversal air flow causes a flow resistance or pressure drop through the anode layer and the coefficient of permeability (α) is recorded using the methodology and relationship described in [16, 17]. Higher α corresponds to better permeability of gas through the layer. The data obtained for conventional nanostructured layers is given in Figure 6. The conductivity of nanostructured and conventional anodes, measured by the 4-point dc method at 800 °C in Ar+5 vol% H₂, was comparable for 50 hours, as shown in Figure 7. An increase in the conductivity of nanostructured anodes was recorded for prolonged dwell times which was associated to coalescence and phase I sintering (neck formation) of Ni particles. The polarization of a conventional and a nanostructured anode was measured during SOFC operation at 800 °C by using impedance spectroscopy and equivalent circuit diagrams. The setup and details of measurements are described elsewhere [18]. With simulated reformat fuel gas (0.5 slm H₂ and 0.5 slm N₂) the polarization measured at open circuit voltage (OCV) associated to the anode was decreased from 0.74 Ωcm^2 for conventional materials to 0.42 Ωcm^2 for the nanostructured layer. Consequently, the cell power density was increased from 230 mW/cm² to 309 mW/cm² after cell activation which typically takes 80 to 100 hours as shown in Figure 8. Please note that during the initial 80 to 100 hours of cell operation cells tested at DLR show an improvement in OCV and a decline in area specific resistance (ASR) leading to a significant increase (almost twice) in cell output power density. The effects, though not fully studied, are associated with the improvement in contacting, sealing and electrode forming [19]. Reliable cell performance data is therefore reported after 100 hours. After 1500 hours of operation a decrease of 5% in the

powder density was calculated. As the metal supported cells of DLR typically show degradation rates between 2.5 and 4.5%/1000 h [20], the 3.33%/1000 h degradation rate of cells consisting of a nanostructured anode did not point towards any additional degradation linked to the use of nanomaterials. However, after 100 hours of operation, the nanostructured anode revealed neck formation and some densification, although the particle size remained comparable to that of the as-sprayed coating which was between 60 and 220 nm, as shown in Figure 9 (a). In a nanostructured anode operated for 1500 hours (Figure 9 (b)), limited particle growth was evident and random measurements on micrographs gave average particle sizes between 95 and 390 nm. This stability of the anode layer can be attributed to the distribution of YSZ and Ni particles inside the anode. While working with plasma sprayed deposits using 8YSZ with a particle size of 40 nm Christenn and Ansar [21] demonstrated that the phase I of sintering does not start in free standing deposits below 932°C at least for 60 hours and in constrained conditions the sintering kinetics for nanostructured YSZ deposit are further slowed. Using these results the nanostructured anode powder and deposit were prepared in a manner to limit percolation of nano-NiO particles. As a result, although the sintering at 800 °C could not be eliminated, it was impeded due to the YSZ particles. The percolation of Ni is, however, mandatory for the electronic conductivity in the anode and the micro-sized NiO was therefore added. Nevertheless, more work is needed to understand the grain growth of nanomaterials at cell operating conditions and the methodology to inhibit it.

Nanostructured anodes using DC Suspension and Solution Precursor Plasma Spraying (SPS and SPPS)

Despite significantly better properties of deposits produced by spraying of agglomerated nanoparticles compared to conventional materials the control of microstructure can be very challenging and the degree of porosity can only be tailored between 5 to 20%. Moreover, as the surface of each agglomerate needs to be melted for adhesion on the substrate a large share of nanoparticles gets entrapped in the molten and re-solidified shell and does not contribute to the electrochemical activity of the electrodes. For functional deposits having a denser or an extremely porous structure of nanomaterials alternative methods are under development in our group. These methods consist of introducing nanoparticles as suspension, called suspension plasma spraying (SPS), or as precursor solutions, referred as solution precursor plasma spraying (SPPS), using DC plasma torches. Besides DLR, several groups have elaborated activities in these processing techniques [22, 23, 24]. The former method uses nanoparticles dispersed in a solvent as feedstock. The preparation of this suspension is a crucial step of the process. The goal of the preparation is to avoid agglomeration of the particles to attain homogeneous distribution of the particles required for constant feed rate and reduced sedimentation. As the Van-der-Waals forces are the major cause of the agglomeration, the suspensions are stabilized by promoting inter-particle repulsion by stearic or electrostatic repulsion [25]. Zeta-potential (ζ) is a common tool to measure the stability of suspensions. During the radial injection in the DC plasma, the solvent around the particles increases their momentum, as the mass of a droplet containing nanoparticles is several orders of magnitude higher than the mass of an individual nanoparticle. This assists in delivering the particles till the core of the plasma jet. During the flight in the

plasma jet the solvent evaporates and releases the nanoparticles which are then melted and accelerated towards the substrate. In solution precursor plasma spraying a solution of the target material, usually nitrates, chlorates or sulfates, is injected into the plasma flame. Inside the flame the solvent evaporates and the precursor materials react and calcinate. Depending on the plasma process and the operating conditions the deposit is generated either by growth from the vapor phase or after melting and impingement of particles on the substrate. As both processes are based on the injection of liquid feedstock a very similar system can be used. In this work suspension plasma spraying was conducted by a DC-TriplexPro gun from Sulzer Metco, Switzerland, using either atomizing or solid stream nozzles as shown in Figure 10. The powders were nanosized 8YSZ and NiO from Marion Technology, France (11 (a)). The average particle size of 8YSZ was 35 nm whereas for NiO it was 92 nm. The suspensions were prepared in water using appropriate dispersants (Figure 11(b)). Typical micrographs for very low and extremely high porosity are shown in Figure 12 (a) and (b), respectively. Along with 45 nm particles in 12 (b), a larger splat can be observed. It is believed to form when droplets trajectory is through a cooler plasma zone causing slow evaporation of the solvent. Agglomeration of nanoparticles thus takes place and the formed agglomerate then melts and impacts as single larger particle forming a splat with epitaxial crystals. For the dc solution precursor plasma spraying aqueous solutions of zirconyl nitrate and yttrium nitrate from Alfa Aesar, France, were prepared. The ratio of the two components were adjusted to have 8 mole% Y_2O_3 in the deposit. Solid loading was from 5 to 30 wt.%. The solution was injected in the TriplexPro gun using an atomizing nozzle. The resulting coating was highly porous (Figure 13) having the cubic phase of zirconium oxide as checked by XRD.

Conclusion

The paper has given an overview about the advances in plasma spray processes to manufacture nanostructured functional layers for the application in SOFC. Improvement in cell performance was attempted by introducing nanostructured deposits as electrodes while maintaining acceptable degradation rates. Two major cost-effective approaches have been described. In the first one in-situ synthesis and deposition of nanostructured cathodes from liquid solution precursors was performed in an inductively coupled RF plasma. The cathodes initially exhibited undesirable secondary phases. This problem was overcome by adjusting the chemical composition of the precursors and controlling the thermally activated volatility of species during RF plasma in-flight. The deposit microstructure was columnar type with very high open porosity and specific surface area which can offer excellent performance in SOFC. In the second approach nanomaterials were pre-synthesized and introduced in a DC plasma as agglomerates or suspensions. The pre-synthesized nanoparticles had a size of 40 to 90 nm and the particles size was mostly conserved after spraying; some portion was melted in-flight to provide adhesion on the substrate which leads to the incorporation of micro-sized particles. By performing electrochemical and impedance spectroscopy measurements it was found that the nanostructured anode had 43.2% lower polarization (at OCV) in SOFC operation (800 °C; 0.5 slm H₂ and 0.5 slm N₂ mixture as fuel gas) compared to conventional anodes. This resulted in a power density of 309 mW/cm² for cells consisting of nanostructured anodes which is 34.5% higher than that of cells with conventional plasma sprayed anodes. Moreover, by controlling the electrode structure only limited growth in the nano-sized particles of the anode was observed after 1500 hours of operation at 800 °C. In as-sprayed nanostructured anodes and anodes after 100 hours of operation the

particle size was between 60 and 220 nm whereas it was between 95 and 390 nm after 1500 hours of operation. Further improvement in the microstructure of anodes is in progress using dc plasma suspension and solution precursor spraying

Acknowledgment

The experimental work on TPCVD performed by Dr. Matthias Müller during the period of his PhD is gratefully acknowledged. The authors would also like to thank Ms. Zeynep Ilhan for conducting the electrochemical tests.

References

1. Kendall, K., Singhal, S.C., 2003. High Temperature Solid Oxide Fuel Cells: Fundamentals, Design and Applications. Elsevier, Amsterdam..
2. Minh N.Q., Takahashi T., 1995. Science and Technology of Ceramic Fuel Cells. Elsevier, Amsterdam.
3. Chen, J., Kim, J.W., Tanner C:W., Virkar,A.V , 2000. The role of electrode microstructure on activation and concentration polarization in solid oxide fuel cells. Solid State Ionics 131, 189-198.
4. Kenjo, T., Nishiya, M., 1992. LaMnO₃ air cathodes containing ZrO₂ electrolyte for high temperature solid oxide fuel cells. Solid State Ionics 57, 295-302.
5. Abeles, B., Deng, H., Zhou, M., 1994. Diffusion-reaction in mixed ionic-electronic solid oxide membranes with porous electrodes. Solid State Ionics 74, 75-84.

6. Arnold, J., Ilhan, Z., Schiller, G., Syed, A.A., Weckmann, H., 2006. Improving plasma sprayed YSZ coatings for SOFC electrolytes. *J. Therm. Spray. Technol.* 15(4), 617-622
7. Tuller H.L., 2000. Ionic conduction in nanocrystalline materials. *Solid State Ionics*, 131, 143-157
8. Maier, J., 2002. Nano-sized mixed conductors (Aspects of nano-ionics. Part III). *Solid State Ionics*, 148, 367-374.
9. Thermal spraying, 1985. American Welding Soc., Miami, USA
10. Davis, J.R. (ed.), 2004. Handbook of thermal spray technology. ASM International, USA.
11. Denoirjean A., Denoirjean P., Fauchais, P., Hannover, B., Khan, A.A., Labbe, J.C., Syed, A.A., 2005. Influence of substrate surface conditions on the plasma sprayed ceramic and metallic particles flattening. *Surf. Coat. Technol.*, 200, 2317-2331.
- 12 Denoirjean, A., Denoirjean, P., Fauchais, P., Labbe, J.C., Syed, A.A., 2004. Investigation of phenomena influencing properties of plasma sprayed ceramic-metal composite deposits. *J. High Temp. Mater. Proc.* 8 (2), 253- 272.
13. Gitzhofer, F., Müller, M., Schiller, G., 1999. Preparation of perovskite powders and coatings by radio frequency suspension plasma spraying. *J. Thermal Spray Technol.* 8 (3), 1999, 389-392.
14. Bouyer, E., Bradke, M., Branston, D.W., Heimann, R.B., Henne, R., Lins, G., Müller, M., Schiller, G., 2002. Thermal induction plasma processes for the synthesis of SOFC materials. *Materialwissenschaft und Werkstoffkunde* 33 (6), 322-330

15. Henne, R., Lang, M., Ruckdäschel, R., Schaper, S., Schiller, G., 2000. Development of vacuum plasma sprayed thin-film SOFC for reduced operating temperature. *Fuel Cells Bulletin*, 21, 7-12.
16. DIN ISO 4022, 1990. Permeable sinter metals - evaluation of the specific permeability. Berlin (in German)
17. Mould list, 2005. High porous sintered bronze. Publication of GKN Sinter Metals, Radevormwald, Germany
18. Ansar, A., Ilhan, Z., Richter, W., 2007. Synthesis and properties of nanostructured SOFC anode deposits. *J. High Temp. Mater. Proc.* 11 (1), 83 – 94.
19. Arnold, J., Ilhan, Z., Syed, A., Weckmann, H., 2006. Development of Porous Anode Layers for the Solid Oxide Fuel Cell by Plasma Spraying. *J. Therm. Spray Technol.* 15 (4), 604-609.
20. Ansar, A., Arnold, J., Ilhan, Z., 2009. Plasma sprayed metal supported SOFCs having enhanced performance and durability. *J. Therm. Spray. Technol.*, accepted.
21. Ansar, A., Christenn, C., 2009. Investigation of Plasma Sprayed and Constrained-Sintered Zirconia Based Electrolytes, *J. Therm. Spray. Technol.*, accepted
22. Coudert, J.F., Etchart-Salas, R., Fauchais, P. Montavon, G., Rat, V., 2008. Operating parameters for suspension and solution plasma-spray coatings. *Surf. Coat. Technol.* 202 (18), 4309-4317.
23. Babu, K.S., Brinley, E., Seal, S., 2007. The solution precursor plasma spray processing of nanomaterials. *J. of the Minerals* 59 (7), 54-59.
24. Gitzhofer, F., Jia, L., 2008. Induction plasma technology applied to materials synthesis for SOFC. *Int. J. Appl. Ceram. Technol.* 5(6), 537-547.

25. Hofmann, T., 2004. Die Welt der vernachlässigten Dimensionen: Kolloide. Chemie in unserer Zeit, 38, 24.

Figure Captions

Figure 1: Experimental set-up, detail in left corner: principle of gas-assisted atomization

Figure 2: XRD patterns of a TPCVD coating of LSM (precursor A); top: centre, bottom: margin of the sample

Figure 3: XRD patterns of a TPCVD coating of PSCF (precursor H), top: centre, bottom: margin of the sample.

Figure 4: SEM images of a fracture surface of a TPCVD perovskite coating

Figure 5: SEM of the agglomerated nanostructured 22/78 wt% NiO and YSZ powder (a) and of the fractured cross section of the produced deposit after spraying of this powder (b).

Figure 6: Comparison of permeability coefficient of conventional and nanostructured anodes.

Figure 7: Conductivity of nanostructured anode in Ar- 5 vol% H₂ at 800°C as a function of time along with a comparison of conductivity of conventional and nanostructured anodes for 35 hrs. .

Figure 8: U(i) curves of reference cell (□), cell with nanostructured anode after 100 h (Δ) and after 1500 h of operation (◇) at 800°C (area 12.6 cm²; 0.5 slm H₂+0.5 slm N₂/2.0 slm air).

Figure 9: SEM micrographs (2000X) of nanostructured anode after 100 h and 1500 h of SOFC operation. Micrograph (1000X) of as-sprayed deposit is given in Figure 5 (b).

Figure 10: Inverted photo of atomizing nozzle (a) and picture of liquid injection by a solid stream nozzle into the plasma (b)

Figure 11: SEM image of the 8YSZ nanopowder (a) and typical zeta-potential measurement for suspension stabilization with increasing amount of dispersant (b).

Figure 12: Micrograph of thin dense (a) and highly porous (b) nanostructured YSZ deposits produced for SOFC by Suspension Plasma Spraying.

Figure 13: SEM images of porous zirconia layer by solution precursor plasma spraying.

Tables

Table 1: Summary of the precursor solutions applied and the desired synthesis products

Table 2: Phase purity of different TPCVD perovskite coatings

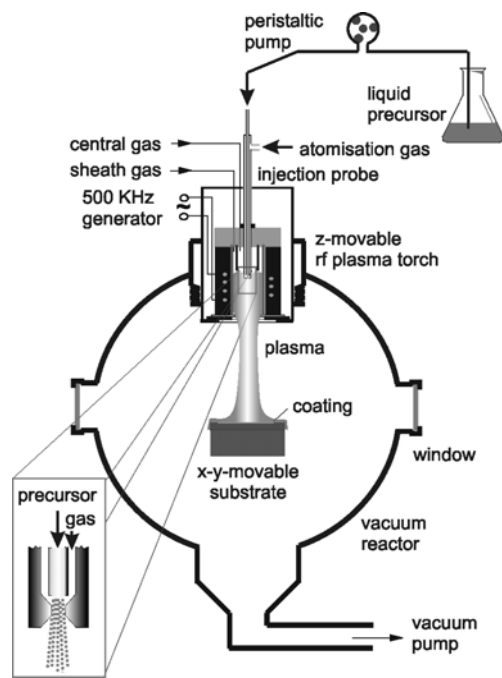


Figure 1: Experimental set-up, detail in left corner: principle of gas-assisted atomization

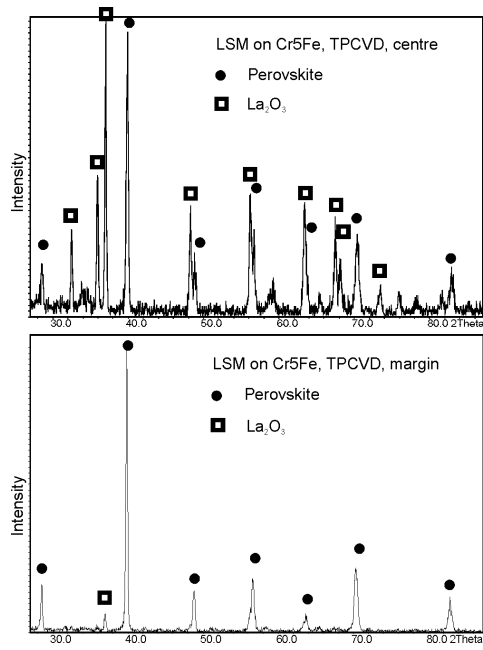


Figure 2: XRD patterns of a TPCVD coating of LSM (precursor A); top: centre, bottom: margin of the sample

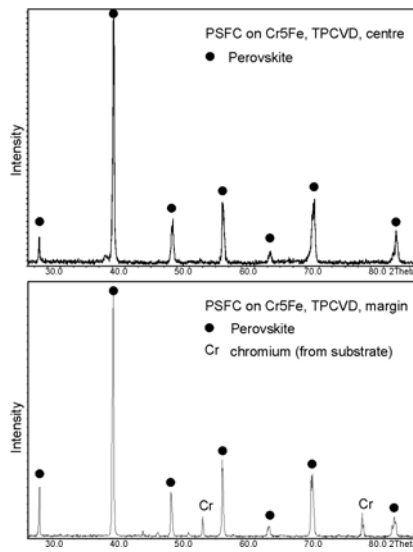


Figure3: XRD patterns of a TPCVD coating of PSFC (precursor H), top: centre, bottom: margin of the sample.

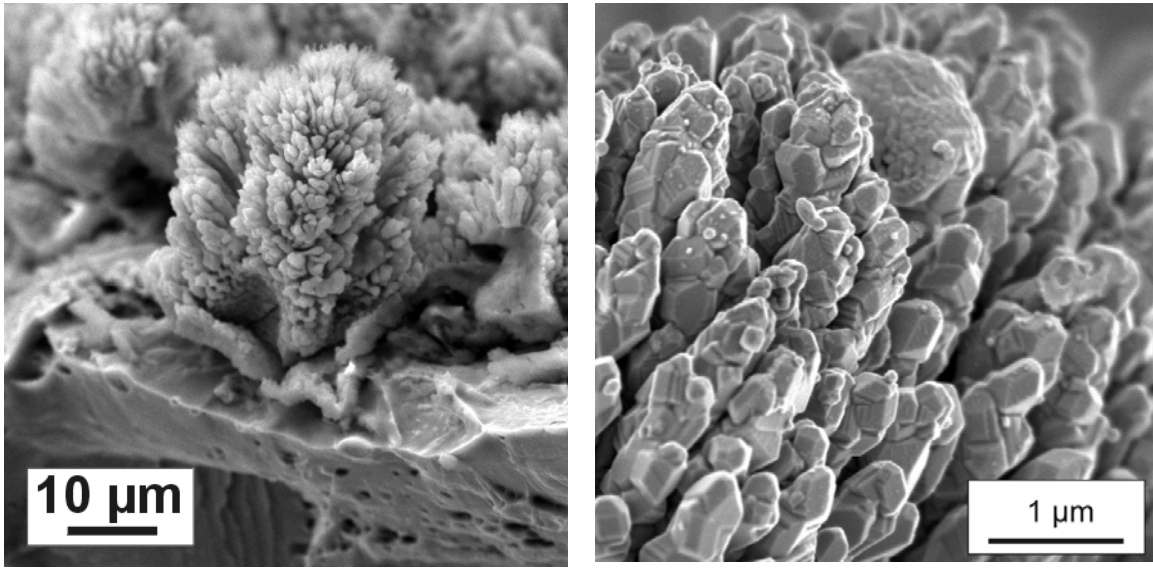
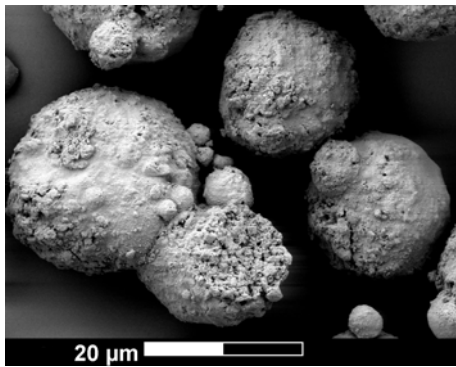
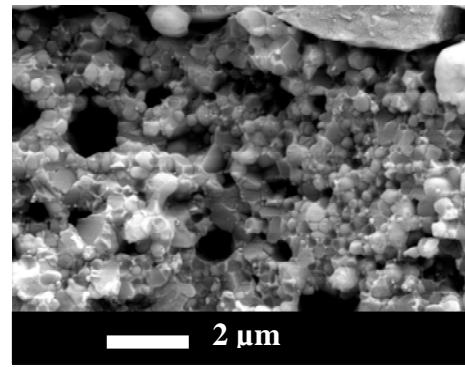


Figure 4: SEM images of a fracture surface of a TPCVD perovskite coating



(a)



(b)

Figure 5: SEM of the agglomerated nanostructured 22/78 wt% NiO and YSZ powder (a) and of the fractured cross section of the produced deposit after spraying of this powder (b).

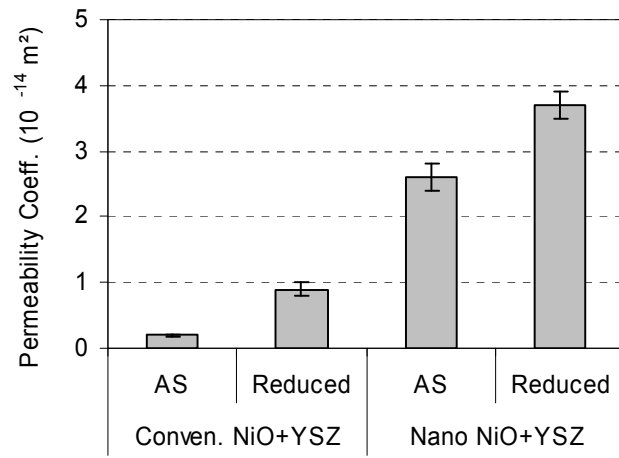


Figure 6: Comparison of permeability coefficient of conventional and nanostructured anodes.

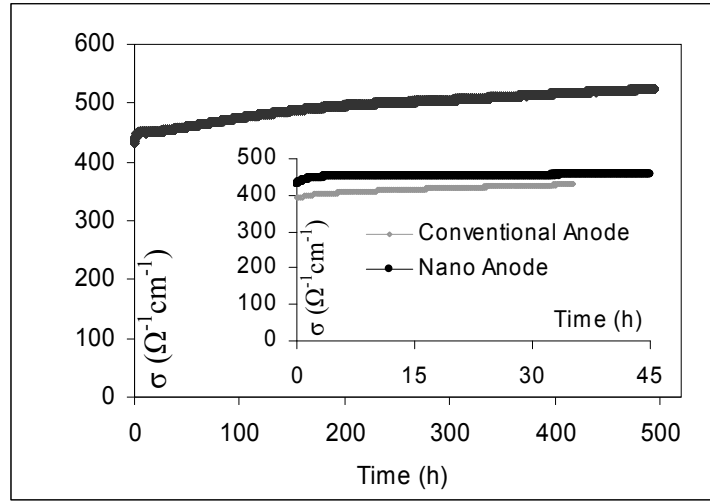


Figure 7: Conductivity of nanostructured anode in Ar- 5 vol% H₂ at 800°C as a function of time along with a comparison of conductivity of conventional and nanostructured anodes for 35 hrs. .

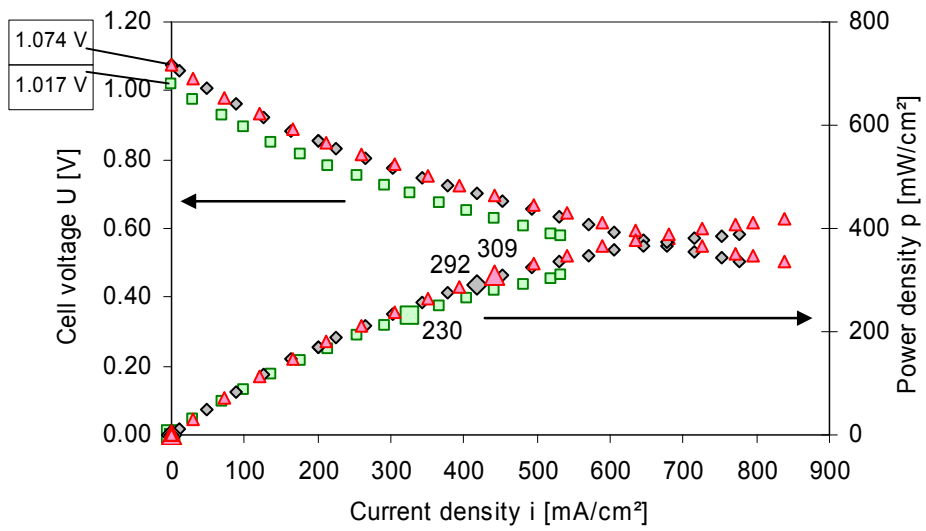


Figure 8: $U(i)$ curves of reference cell (\square), cell with nanostructured anode after 100 h (Δ) and after 1500 h of operation (\diamond) at 800°C (area 12.6 cm^2 ; $0.5 \text{ slm H}_2 + 0.5 \text{ slm N}_2 / 2.0 \text{ slm air}$).

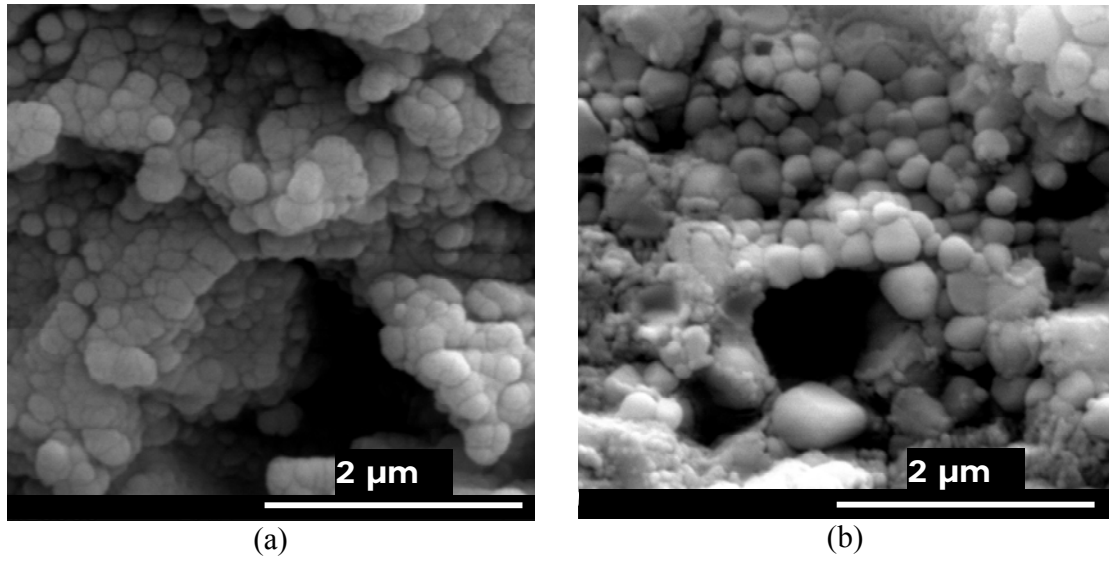


Figure 9: SEM micrographs (2000X) of nanostructured anode after 100 h and 1500 h of SOFC operation. Micrograph (1000X) of as-sprayed deposit is given in Figure 5 (b).

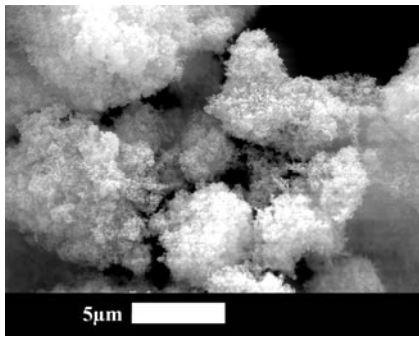


(a)

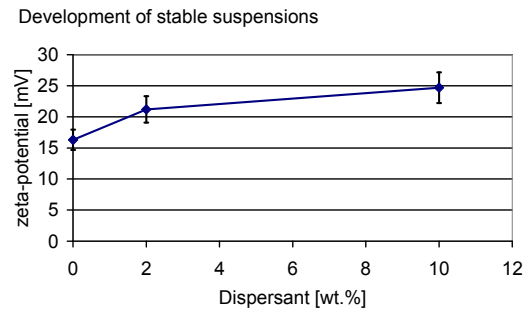


(b)

Figure 10: Inverted photo of atomizing nozzle (a) and picture of liquid injection by a solid stream nozzle into the plasma (b)

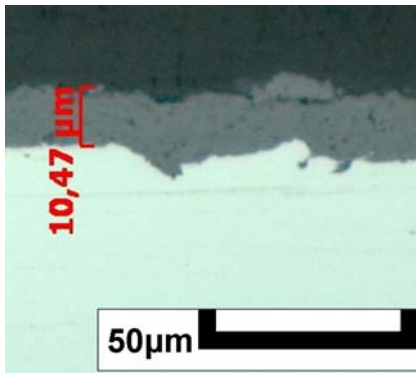


(a)

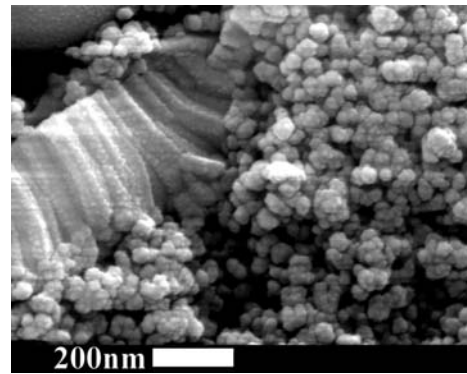


(b)

Figure 11: SEM image of the 8YSZ nanopowder (a) and typical zeta-potential measurement for suspension stabilization with increasing amount of dispersant (b).



(a)



(b)

Figure 12: Micrograph of thin dense (a) and highly porous (b) nanostructured YSZ deposits produced for SOFC by Suspension Plasma Spraying.

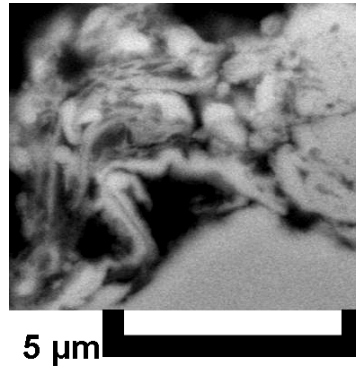
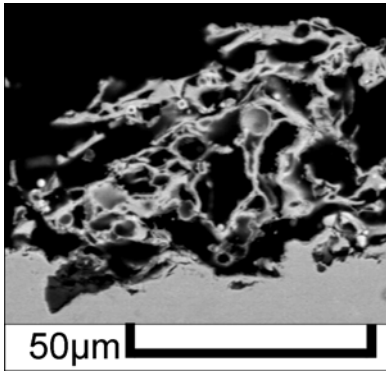


Figure 13: SEM images of porous zirconia layer by solution precursor plasma spraying.

Tables

	Synthesis product	Precursor	Concentration
A	$\text{La}_{0,9}\text{Sr}_{0,1}\text{MnO}_3$ (LSM)	$\text{La}(\text{NO}_3)_3 \cdot 6 \text{H}_2\text{O}$ $\text{Sr}(\text{NO}_3)_2$ $\text{Mn}(\text{NO}_3)_2 \cdot 4 \text{H}_2\text{O}$	0,9 M 0,1 M 1,0 M
B	$\text{La}_{0,5}\text{Sr}_{0,5}\text{MnO}_3$ (LSM)	$\text{La}(\text{NO}_3)_3 \cdot 6 \text{H}_2\text{O}$ $\text{Sr}(\text{NO}_3)_2$ $\text{Mn}(\text{NO}_3)_2 \cdot 4 \text{H}_2\text{O}$	0,5 M 0,5 M 1,0 M
C	$\text{La}_{0,65}\text{Sr}_{0,3}\text{MnO}_3$ (ULSM)	$\text{La}(\text{NO}_3)_3 \cdot 6 \text{H}_2\text{O}$ $\text{Sr}(\text{NO}_3)_2$ $\text{Mn}(\text{NO}_3)_2 \cdot 4 \text{H}_2\text{O}$	0,65 M 0,3 M 1,0 M
D	$\text{Pr}_{0,65}\text{Sr}_{0,3}\text{MnO}_3$ (UPSM)	$\text{Pr}(\text{NO}_3)_3 \cdot 5 \text{H}_2\text{O}$ $\text{Sr}(\text{NO}_3)_2$ $\text{Mn}(\text{NO}_3)_2 \cdot 4 \text{H}_2\text{O}$	0,65 M 0,3 M 1,0 M
E	$\text{La}_{0,8}\text{Sr}_{0,2}\text{FeO}_3$ (LSF)	$\text{La}(\text{NO}_3)_3 \cdot 6 \text{H}_2\text{O}$ $\text{Sr}(\text{NO}_3)_2$ $\text{Fe}(\text{NO}_3)_3 \cdot 9 \text{H}_2\text{O}$	0,8 M 0,2 M 1,0 M
F	$\text{La}_{0,8}\text{Sr}_{0,2}\text{Co}_{0,5}\text{Fe}_{0,5}\text{O}_3$ (LSCF)	$\text{La}(\text{NO}_3)_3 \cdot 6 \text{H}_2\text{O}$ $\text{Sr}(\text{NO}_3)_2$ $\text{Co}(\text{NO}_3)_2 \cdot 6 \text{H}_2\text{O}$ $\text{Fe}(\text{NO}_3)_3 \cdot 9 \text{H}_2\text{O}$	0,8 M 0,2 M 0,5 M 0,5 M
G	$\text{La}_{0,58}\text{Sr}_{0,4}\text{Co}_{0,2}\text{Fe}_{0,8}\text{O}_3$ (LSCF)	$\text{La}(\text{NO}_3)_3 \cdot 6 \text{H}_2\text{O}$ $\text{Sr}(\text{NO}_3)_2$ $\text{Fe}(\text{NO}_3)_3 \cdot 9 \text{H}_2\text{O}$ $\text{Co}(\text{NO}_3)_2 \cdot 6 \text{H}_2\text{O}$	0,58 M 0,4 M 0,8 M 0,2 M
H	$\text{Pr}_{0,58}\text{Sr}_{0,4}\text{Co}_{0,2}\text{Fe}_{0,8}\text{O}_3$ (PSCF)	$\text{Pr}(\text{NO}_3)_3 \cdot 5 \text{H}_2\text{O}$ $\text{Sr}(\text{NO}_3)_2$ $\text{Fe}(\text{NO}_3)_3 \cdot 9 \text{H}_2\text{O}$ $\text{Co}(\text{NO}_3)_2 \cdot 6 \text{H}_2\text{O}$	0,58 M 0,4 M 0,8 M 0,2 M

Table 1: Summary of the precursor solutions applied and the desired synthesis products

Precursor	ULSM		UPSM		LSCF		PSCF	
Position	centre	margin	centre	margin	centre	margin	centre	margin
Phase purity	85 %	100 %	92 %	100 %	65 %	100 %	100 %	100 %

Table 2: Phase purity of different TPCVD perovskite coatings